

First-principles Modelling of SrTiO₃ based Oxides for Thermoelectric Applications

Daniel I. Bilc, Calin G. Floare, Liviu P. Zârbo, Sorina Garabagiu

Mol & Biomol Phys Dept, Natl Inst Res & Dev Isotop& Mol Technol, RO-400293 Cluj-Napoca

Sebastien Lemal, and Philippe Ghosez

*Physique Théorique des Matériaux, Q-MAT, CESAM,
Université de Liège (B5), B-4000 Liège, Belgium*

Using first-principles electronic structure calculations, we studied the electronic and thermoelectric properties of SrTiO₃ based oxide materials and their nanostructures identifying those nanostructures which possess highly anisotropic electronic bands. We showed recently that highly anisotropic flat-and-dispersive bands can maximize the thermoelectric power factor, and at the same time they can produce low dimensional electronic transport in bulk semiconductors. Although most of the considered nanostructures show such highly anisotropic bands, their predicted thermoelectric performance is not improved over that of SrTiO₃. Besides highly anisotropic character, we emphasize the importance of the large weights of electronic states participating in transport and the small effective mass of charge carriers along the transport direction. These requirements may be better achieved in binary transition metal oxides than in ABO₃ perovskite oxide materials.

PACS numbers:

I. INTRODUCTION

Thermoelectric (TE) technology exploits the ability of certain materials for direct and reversible conversion of thermal energy into electricity. This double edge ability gives TE technology a strong appeal in almost all energy-related applications. Nevertheless, many fundamental problems have to be solved and in particular the intrinsic efficiency of TE materials still needs to be significantly improved before TE technology becomes a competitive alternative. The efficiency of a TE material depends on the dimensionless figure of merit, $ZT = (S^2\sigma T)/\kappa_{th}$, where σ is the electrical conductivity, S is the thermopower or Seebeck coefficient, T is the absolute temperature, κ_{th} is the total thermal conductivity including electronic and lattice contributions, and $S^2\sigma$ is the power factor (PF). Improving TE efficiency is not obvious because the parameters entering ZT are interlinked, and cannot be optimized independently. Moreover, ZT has to be optimized in a T range at which the TE devices will operate. Many interesting TE applications function at high T , and for practical applications other aspects are also very important such as: the cost of materials, their stability at high T , their toxicity, and availability.

Oxide materials are not known to exhibit the highest TE performance, but they offer stability in oxidizing and corrosive environments at high T ($T > 800 - 1000$ K). In this context, oxides appear very appealing for high T applications. Consequently, efforts have been devoted over the last 15 years to the optimization of TE properties of both n-type and p-type oxide materials. Good candidates for n-type materials include Nb-, W-, La-, Ce-, Pr-, Nd-, Sm-, Gd-, Dy-, and Y-doped SrTiO₃ [1–13], Nb-, La-, Nd-, Sm-, and Gd-doped Sr₂TiO₄, and Sr₃Ti₂O₇ [14], La-doped CaMnO₃ [15] or Al-, Ge-, Ni- and Co-doped ZnO [16–20], Ce-doped In₂O₃ [21], Er-doped CdO [22, 23], TiO₂ [24], Nb₂O₅ [24],

WO₃ [24], while for p-type materials the most promising compounds are Ca₃Co₄O₉ [25] with $ZT \sim 0.3$ at 1000 K [26], and BiCuSeO with $ZT \sim 1.4$ at 923 K.[27] Many studies have concerned doped SrTiO₃, demonstrating the largest $ZT \sim 0.4$ in SrTi_{0.8}Nb_{0.2}O₃ films at 1000 K [2], and $ZT \sim 0.41$ in bulk Sr_{1-3x/2}La_xTiO₃ at 973 K.[12] Different strategies have been proposed to further increase TE efficiency. Attempts to decrease the lattice thermal conductivity κ_l by atomic substitution of Sr by Ba have been envisaged but seem to negatively affect the TE performance.[28] A more promising approach is the reduction of κ_l from scattering of phonons at interfaces, highlighted in layered Ruddlesden-Popper (RP) compounds. [29] Also, Ohta *et al.* demonstrated significant enhancement of S arising from electron confinement and the formation of two dimensional electron gas (2-DEG) in SrTiO₃/Nb-SrTiO₃ superlattices.[26] Although very promising, the inactive SrTiO₃ interlayer must be sufficiently large to avoid electron tunneling and to get significant enhancement of S [30], but this decreases the effective TE performance. In order to maximize TE performance, we showed that the 2-DEG has to be achieved in doped semiconducting nanostructures rather than those with metallic character.[31] Few first-principles studies have investigated the electronic properties of Nb-doped SrTiO₃ [32–34] and Sr₂TiO₄ [35] and a few studies have addressed TE properties of SrTiO₃ [36–44], BaTiO₃ [44], PbTiO₃ [45], CaTiO₃ [44], KTaO₃ [46], HoMnO₃ [47], CaMnO₃ [48–51], Ca₃Co₄O₉ [52], ZnO [53–57], Cu₂O [58], CdO [59], TiO₂ [60], and V₂O₅ [61]. At this stage, a complete understanding of the transport properties and moreover of the band structure engineering in oxide materials is still missing.

Employing the concept of electronic band structure engineering and our guidance ideas, we showed recently that very anisotropic flat-and-dispersive electronic bands

are able to maximize the PF and carrier concentration n of bulk semiconductors, and at the same time to produce low-dimensional electronic transport (low-DET).[62] In practice this is typically achieved from the highly directional character of some orbitals like the d states. Transition metal (TM) oxides with d -type conduction states appear as a well suited playground to explore this concept. Also the rich crystal chemistry of oxides encourages strategies of multiscale nanostructuring [63, 64] by considering hybrid crystal structures that contain discrete structural blocks or layers. The nanostructuring of such hybrid materials is possible in order to engineer their electronic band structures and to lower their κ_l . Therefore, in this theoretical work, we studied TE properties of SrTiO₃ based materials and their nanostructures. We have considered the (SrTiO₃)_{*m*}-(LaVO₃)₁ and (SrTiO₃)_{*m*}-(KNbO₃)₁ superlattices (SL). LaVO₃ is a Mott insulator with an electronic band gap $E_g \sim 1.1$ eV [65], which shows a $PF \sim 0.06$ mW/mK² at 1000 K. [66] For (SrTiO₃)_{*m*}-LaVO₃ nanostructures we expect an electronic transport achieved through LaVO₃ layers since it has a smaller band gap than SrTiO₃ ($E_g \sim 3.3$ eV), which may give rise to low-DET and enhanced PF . We consider (SrTiO₃)_{*m*}-KNbO₃ SL in order to compare their results with those of Nb-doped SrTiO₃. We also studied TE properties of Sr and Co based naturally-ordered Ruddlesden-Popper compounds (AO[ABO₃]_{*m*}), which are more easy to control experimentally and more realistic for practical applications than artificial nanostructures.

II. TECHNICAL DETAILS

The structural, electronic and TE properties of considered oxide structures were studied within density functional theory (DFT) formalism using the hybrid functional B1-WC.[67] B1-WC hybrid functional describes the electronic properties (band gaps) and the structural properties with a better accuracy than the usual simple functionals, being more appropriate for correlated materials such as oxides.[67–69] For comparison of bulk SrTiO₃ results, we also used approximations based on LDA [70], GGA(PBE [71] and GGA-WC [72]) usual simple functionals. The electronic structure calculations have been performed using the linear combination of atomic orbitals method as implemented in CRYSTAL first-principles code.[73] We used localized Gaussian-type basis sets including polarization orbitals and considered all the electrons for Ti [74], O [75], V [78], K and Nb [76], F and Co [77]. The Hartree-Fock pseudopotential for Sr [75], and the Stuttgart energy-consistent pseudopotential for La [79] were used.

In order to go beyond the rigid band approximation, we considered $3 \times 3 \times 3$ SrTiO₃ perovskite supercells with $P\bar{1}$ symmetry, which incorporate explicitly two Nb and two La doping elements per supercell. For (SrTiO₃)_{*m*}-(LaVO₃)₁ and (SrTiO₃)_{*m*}-(KNbO₃)₁ nanostructures, we

have considered $a \times a \times c$ SL with $P4mm$ symmetry to treat the nonmagnetic and ferromagnetic (FM) order, and $\sqrt{2}a \times \sqrt{2}a \times c$ SL with $P4bm$ symmetry for the FM and antiferromagnetic (AFM) orders, where a is the lattice constant of cubic perovskite structure. For AO[ABO₃]_{*m*} SL with $I4/mmm$ symmetry the body centered primitive cells were used in calculations. According to the position of F at the apical site, the symmetry of Sr₂CoO₃F has been reduced to $Cmcm$ and $Cmmm$ space groups for type I and type II ordered structures, respectively. For these F ordered structures, we used the face centered primitive cells in our calculations.

Brillouin zone integrations were performed using the following meshes of k -points: $6 \times 6 \times 6$ for bulk SrTiO₃, Sr₂TiO₄, and Sr₂CoO₃F, $3 \times 3 \times 3$ for La and Nb doped $3 \times 3 \times 3$ SrTiO₃ supercells, $6 \times 6 \times 4$ for (SrTiO₃)₁-(LaVO₃)₁ and (SrTiO₃)₁-(KNbO₃)₁ SL, $6 \times 6 \times 1$ for (SrTiO₃)₅-(LaVO₃)₁ and (SrTiO₃)₅-(KNbO₃)₁ SL, and $4 \times 4 \times 4$ for Sr₃Ti₂O₇. The self-consistent-field calculations were considered to be converged when the energy changes between interactions were smaller than 10^{-8} Hartree. An extra-large predefined pruned grid consisting of 75 radial points and 974 angular points was used for the numerical integration of charge density. Full optimizations of the lattice constants and atomic positions have been performed with the optimization convergence of 5×10^{-5} Hartree/Bohr in the root-mean square values of forces and 1.2×10^{-3} Bohr in the root-mean square values of atomic displacements. The level of accuracy in evaluating the Coulomb and exchange series is controlled by five parameters.[73] The values used in our calculations are 7, 7, 7, 7, and 14.

The transport coefficients were estimated in the Boltzmann transport formalism and the constant relaxation time approximation using BoltzTraP transport code.[80] The electronic band structures (energies), used in the transport calculations, were calculated with electronic charge densities converged for denser k -point meshes (doubling the k -point meshes used in optimization calculations). The transport coefficients were very well converged for the energies calculated on k -point meshes of $59 \times 59 \times 59$ for bulk SrTiO₃, Sr₂TiO₄, Sr₃Ti₂O₇, and Sr₂CoO₃F, $27 \times 27 \times 27$ for La doped $3 \times 3 \times 3$ SrTiO₃ supercell, $59 \times 59 \times 41$ for (SrTiO₃)₁-(LaVO₃)₁ and (SrTiO₃)₁-(KNbO₃)₁ SL, and $59 \times 59 \times 23$ for (SrTiO₃)₅-(LaVO₃)₁ and (SrTiO₃)₅-(KNbO₃)₁ SL.

The effective masses were obtained by calculating values of energy close to conduction band (CB) minimum and valence band (VB) maximum while moving from the extremum points along the three directions of the orthogonal reciprocal lattice vectors k_i ($i=x, y, z$). The energy values, $\epsilon_{\vec{k}}$, were fitted up to 10-th order polynomials in k_i . In general $\epsilon_{\vec{k}}$ can be expanded about an extremum point as:

$$\frac{2m_e}{\hbar^2} \epsilon_{\vec{k}} = \sum_{i,j} \frac{m_e}{m_{ij}} k_i k_j \quad (1)$$

where m_{ij} are the components of the effective mass tensor

TABLE I: Lattice constant a , and indirect band gap E_g of SrTiO₃ perovskite structure estimated within different functionals. The experimental values are included for comparison.

	LDA	PBE	GGA-WC	B1-WC	Exp.
$a(\text{\AA})$	3.864	3.943	3.898	3.880	3.890 ^a
$E_g(\text{eV})$	2.24	2.25	2.25	3.57	3.25 ^b

^aExtrapolated at 0 K from Ref. [82].

^bFrom Ref. [83].

($i, j=x, y, z$) and m_e is the free electron mass. In the present expansion, we have only the diagonal components of the effective mass tensor m_{ii} , since all the interaxial angles are 90°.

III. RESULTS

The oxide compounds under study are well known to exhibit various types of structural phase transitions with temperature. Since we are interested in TE at high T, in first approximation we restricted our investigation to the high symmetry phases of $Pm\bar{3}m$ for bulk perovskites and $P4mm$, $P4bm$, and $I4/mmm$ for superlattices. Some of them are also expected to show magnetic order at low T and be in a paramagnetic configuration at high T. For the later we compare different magnetic orders to find the systems with lower total energy and more structurally stable.

A. Bulk SrTiO₃ and its alloys

The structural (lattice constant) and electronic (band gap) properties of bulk SrTiO₃ optimized within the different functionals are given in Table I. LDA underestimates the lattice constant and the atomic volume, whereas PBE overestimates these properties, which is the typical behaviour of LDA and PBE functionals. GGA-WC describes very well the structural properties of SrTiO₃, being a functional developed for solids. All the simple functionals underestimate SrTiO₃ band gap, which is an inherent problem of DFT. B1-WC hybrid, which mixes the GGA-WC with a small percentage of exact exchange (16%) describes simultaneously both the structural and electronic properties with good accuracy.

For a more complete theoretical characterization, we have studied also TE properties (σ , S , and PF) of bulk SrTiO₃ within B1-WC hybrid, and the other used simple functionals. In the constant relaxation time approximation, the relaxation time τ is considered as a constant $\tau = \tau_0$ independent of energy and temperature T , and is estimated from fitting of the experimental electrical conductivity σ_{exp} at a given doping carrier concentration n and T . τ within the different functionals was estimated by fitting the room temperature experimental

TABLE II: Relaxation time τ estimated at 300 K within constant relaxation time approximation using different functionals for n-type doped SrTiO₃.

	LDA	GGA-WC	B1-WC
	$\sigma_{exp} = 1.4 \times 10^5 \text{ S/m}, n = 8 \times 10^{20} \text{ cm}^{-3}$		
$\tau(10^{-14} \text{ s})$	0.44	0.46	0.43
	$\sigma_{exp} = 1.667 \times 10^5 \text{ S/m}, n = 1 \times 10^{21} \text{ cm}^{-3}$		
$\tau(10^{-14} \text{ s})$	0.43	0.45	0.42

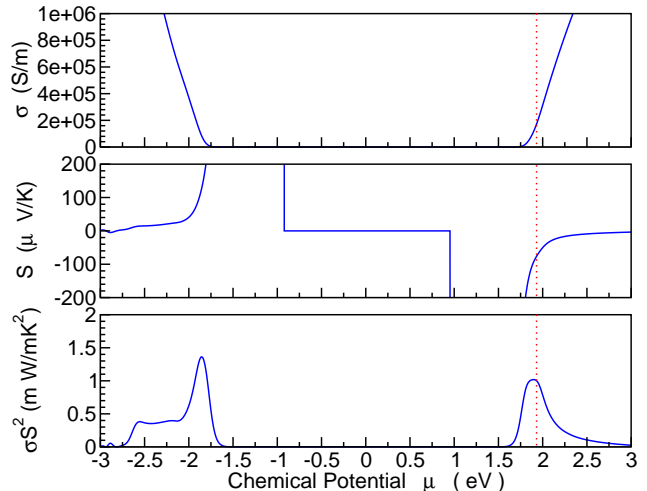


FIG. 1: (Color online) Electrical conductivity σ , Seebeck coefficient S , and power factor $PF = S^2\sigma$ dependence on chemical potential for SrTiO₃ estimated at 300 K within B1-WC using the relaxation time $\tau = 0.43 \times 10^{-14} \text{ s}$. The n-type doping carrier concentration n of $1 \times 10^{21} \text{ cm}^{-3}$ is shown in dashed vertical line.

values $\sigma_{exp} = 1.4 \times 10^5 \text{ S/m}$ at $n = 8 \times 10^{20} \text{ cm}^{-3}$ [81], and $\sigma_{exp} = 1.667 \times 10^5 \text{ S/m}$ at $n = 1 \times 10^{21} \text{ cm}^{-3}$ [2] (Table 2). The resulting value of τ is $\sim 0.43 \times 10^{-14} \text{ s}$, which very similar in all the used functionals (see Table II). The estimated values of σ , S , and PF at 300 K as a function of chemical potential within B1-WC hybrid are given in Fig. 1. For n-type doping, PF is $\sim 1 \text{ mW/mK}^2$, being underestimated with respect to experiment ($PF_{exp} \sim 3 \text{ mW/mK}^2$). [2, 81] This underestimation of PF is due to a low value of thermopower $S \sim -77 \mu\text{V/K}$ in comparison with the experimental value of $S_{exp} \sim -147 \mu\text{V/K}$ at $n = 1 \times 10^{21} \text{ cm}^{-3}$ and 300 K. PF estimated within the usual simple functionals (LDA, GGA-WC) has the same value $\sim 1 \text{ mW/mK}^2$ (Fig. 2).

The promising TE properties of SrTiO₃ based oxides were found for strong n-type doping ($n \sim 10^{21} \text{ cm}^{-3}$, carrier concentrations which are more than one order of magnitude higher than those of typical TE materials such as PbTe, Bi₂Te₃). At these high concentrations, the underestimation of PF within all considered functionals may be generated by the incomplete validity of rigid band structure approximation (Fig. 2). In order to check this, we have considered $3 \times 3 \times 3$ SrTiO₃ supercells which explicitly incorporate La and Nb doping elements, and

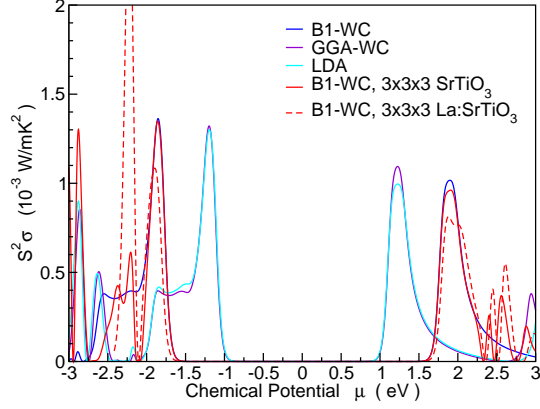


FIG. 2: (Color online) Power factor $PF = S^2\sigma$ dependence on chemical potential for SrTiO_3 estimated at 300 K within different functionals using the relaxation time $\tau = 0.43 \times 10^{-14}$ s. The different PF peak positions within GGA-WC and LDA are due to lower band gap E_g values. PF for $3 \times 3 \times 3$ SrTiO_3 , and La:SrTiO_3 supercells, estimated at 300 K within B1-WC, are also shown.

studied their structural, electronic and transport properties. These doping elements introduce one electron to the systems, and change also the electronic states close to the Fermi level (chemical potential) with respect to that of bulk SrTiO_3 (see the density of states DOS from Fig. 3(a) and (b)). Indeed at these high electronic concentrations the rigid band structure approximation is not completely valid.

We studied TE properties of $3 \times 3 \times 3$ SrTiO_3 supercells, which include explicitly La doping elements ($3 \times 3 \times 3$ La:SrTiO_3). The relaxation time determined by fitting σ_{exp} at $n = 1 \times 10^{21} \text{ cm}^{-3}$ and 300 K is the same as that of bulk SrTiO_3 ($\tau = 0.45 \times 10^{-14}$ s). Although the electronic states near the Fermi level of $3 \times 3 \times 3$ La:SrTiO_3 supercell are slightly different than those of bulk SrTiO_3 at high values of $n = 1.2 \times 10^{21} \text{ cm}^{-3}$ (Fig. 3(b)), PF is comparable with that of bulk SrTiO_3 (Fig. 2). Therefore, the underestimation of experimental power factors PF_{exp} of $\sim 2\text{-}3 \text{ mW/mK}^2$ [2, 81, 84] is not due to the change of electronic states close to Fermi level generated by doping. Kinaci *et al.* also showed that La, Nb and Ta doping do not change significantly the electronic states close to the Fermi level, and TE properties of SrTiO_3 alloys are comparable with those of bulk SrTiO_3 . [38] S values for SrTiO_3 alloys are slightly lower, whereas σ values are slightly larger than those of bulk SrTiO_3 . [38] These results suggest that PF of SrTiO_3 alloys is not expected to increase significantly with respect to that of bulk SrTiO_3 .

We assign the underestimation of PF_{exp} to the enhancement of carrier effective mass due to the electron-phonon coupling interaction, which is compatible with the fact that the electronic transport in n-type SrTiO_3 has a polaronic nature. [85] A factor of 3 larger inertial effective mass m_i^* was obtained from experimental optical conductivity relative to the theoretical m_i^* value of $\sim 0.63m_e$ estimated within LDA. [85] At a given carrier

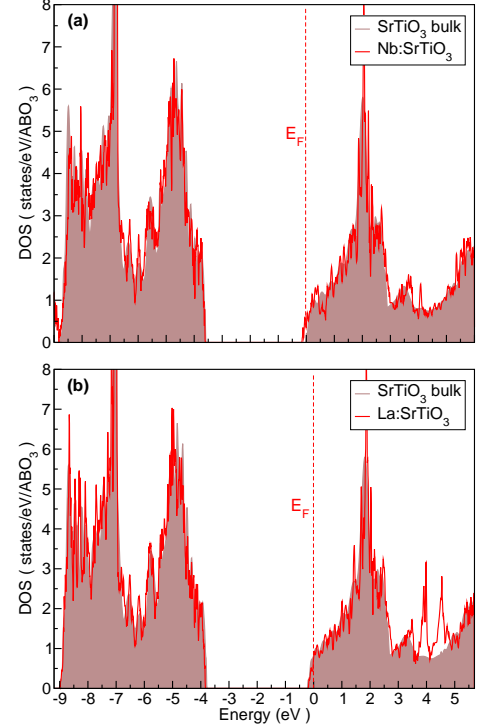


FIG. 3: (Color online) Density of states (DOS) of: (a) Nb doped SrTiO_3 (Nb:SrTiO_3), and (b) La doped SrTiO_3 (La:SrTiO_3) at electronic concentrations $n \sim 1.2 \times 10^{21} \text{ cm}^{-3}$. The Fermi energy E_F is shown in red dashed line. DOS of bulk SrTiO_3 is shown in background brown color.

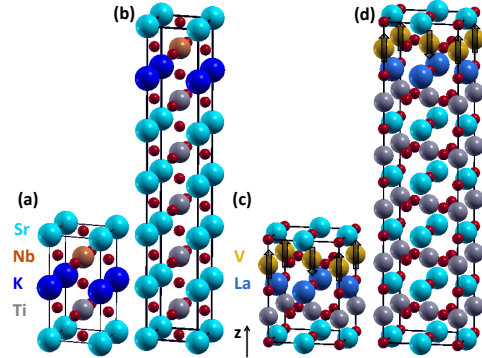


FIG. 4: (Color online) (a)-(b) $(\text{SrTiO}_3)_m(\text{KNbO}_3)_1$ nanostructures with nonmagnetic ground state ($m=1,5$), and (c)-(d) $(\text{SrTiO}_3)_m(\text{LaVO}_3)_1$ nanostructures with AFM ground state ($m=1,5$). The AFM spin order on V atoms is shown by arrows.

concentration, larger experimental effective masses generate larger S_{exp} by lowering the chemical potential relative to CB bottom. We have estimated m_i^* according to the relation [86]:

$$\frac{1}{m_i^*} = \frac{1}{3} \left(\frac{2}{m_l} + \frac{1}{m_h} \right) \quad (2)$$

$0.40m_e(0.39m_e)$, $6.09m_e(6.1m_e)$, and $0.58m_e(0.57m_e)$ where m_l and m_h are the light and heavy effective masses

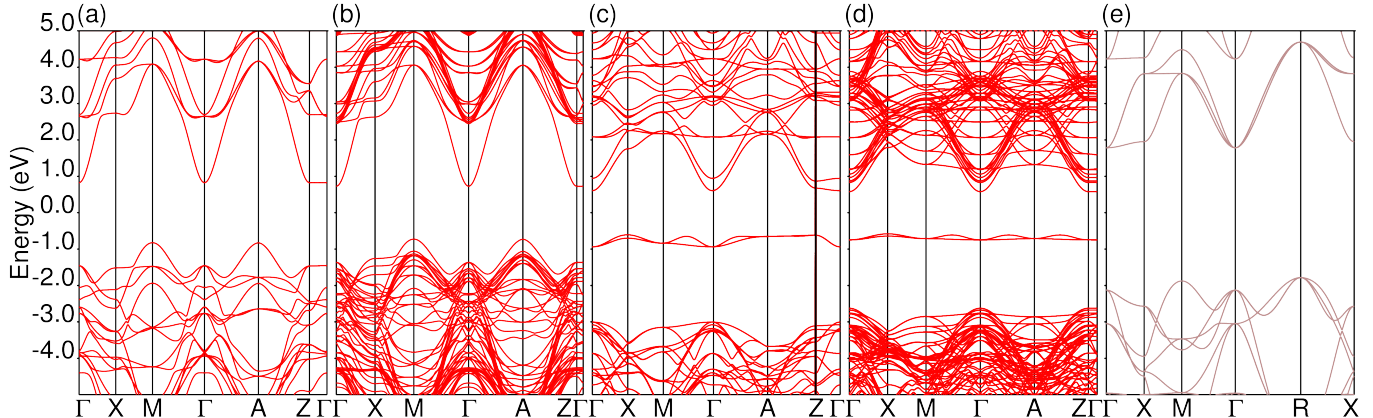


FIG. 5: Electronic band structure of: (a) $(\text{SrTiO}_3)_1(\text{KNbO}_3)_1$, (b) $(\text{SrTiO}_3)_5(\text{KNbO}_3)_1$, (c) $(\text{SrTiO}_3)_1(\text{LaVO}_3)_1$, (d) $(\text{SrTiO}_3)_5(\text{LaVO}_3)_1$ superlattices, and (e) bulk SrTiO_3 estimated within B1-WC.

of the three fold degenerate Ti t_{2g} bands which form the CB bottom. The estimated m_l , m_h , and m_i^* values are within B1-WC(LDA), respectively. Since in the transport calculations we do not account for the polaronic nature of SrTiO_3 conductivity, this translate into small values of the estimated relaxation time (see Table II).

B. Band structure engineering in SrTiO_3 based nanostructures

We considered $(\text{SrTiO}_3)_m(\text{KNbO}_3)_1$ and $(\text{SrTiO}_3)_m(\text{LaVO}_3)_1$ SL nanostructures with $m=1, 5$ for which we studied the electronic and transport properties, and described the relation between size of nanostructures and their TE properties by looking at the effect of quantum confinement on PF . $(\text{SrTiO}_3)_m(\text{KNbO}_3)_1$ SL with $m=1, 5$ have a nonmagnetic ground state. Their structures and electronic band structures are shown in Figs. 4(a),(b), and 5(a),(b). In comparison to bulk SrTiO_3 , $(\text{SrTiO}_3)_1(\text{KNbO}_3)_1$ SL possess smaller E_g , and an electronic band which is very flat along ΓZ direction and dispersive in the other orthogonal directions of the Brillouin zone (see Fig. 6(b)). This very flat-and-dispersive band forms the CB bottom and has a Nb d_{xy} orbital character. The electronic states associated to this very anisotropic band, which participate in the electronic transport, have a reduced weight (short ΓZ distance in the Brillouin zone). The weight is proportional with the density of states DOS and the carrier pocket volumes inside of the Brillouin zone. The reduced weight can be seen more easily from DOS scaled to ABO_3 formula unit (f.u.) (see Fig. 7(a)). The electronic states inside of SrTiO_3 band gap have a small weight, which generate in the inplane direction power factors PF_{xx} smaller than that of bulk SrTiO_3 (Fig. 8(a)). In the cross plane direction, $(\text{SrTiO}_3)_1(\text{KNbO}_3)_1$ SL show large power factors PF_{zz} but at very high n values (chemical potential $\mu \sim 2.75$ eV) which can not be achieved in

experiment. Increasing the quantum confinement in the case of $(\text{SrTiO}_3)_5(\text{KNbO}_3)_1$ SL, decreases the weight of very anisotropic flat-and-dispersive Nb d band. The decrease in weight of this anisotropic band can be seen from the electronic band structure and DOS (see Figs. 5(b), 7(a)), and produces a PF drop relative to $(\text{SrTiO}_3)_1(\text{KNbO}_3)_1$ SL (Fig. 8(a)).

SL formed by $(\text{SrTiO}_3)_m(\text{LaVO}_3)_1$ with $m=1, 5$ have an antiferromagnetic (AFM) ground state. Their structures and electronic band structures are shown in Figs. 4(c),(d), and 5(c),(d). These SL possess two electronic bands laying inside of SrTiO_3 band gap, which are very flat in ΓA and AZ directions, and weakly dispersive in the other directions of Brillouin zone (Fig. 6(b)).

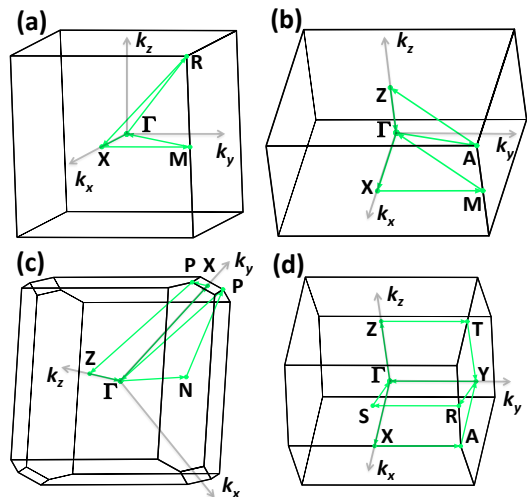


FIG. 6: (Color online) Brillouin zone of: (a) simple cubic SrTiO_3 , (b) tetragonal $(\text{SrTiO}_3)_m(\text{KNbO}_3)_1$ and $(\text{SrTiO}_3)_m(\text{LaVO}_3)_1$ SL ($m=1,5$), (c) body centered tetragonal $\text{SrO}[\text{SrTiO}_3]_m$ ($m=1, 2$), and (d) one face centered tetragonal $\text{Sr}_2\text{CoO}_3\text{F}$ (ground state structure from Fig. 9(c)). The high symmetry points along the directions used in electronic band structures, and the orthogonal reciprocal k_i vectors ($i=x,y,z$) are also shown.

These flat bands create a narrow energy distribution with a very large weight on the top of valence band, being generated by $V d_{xz}$ and d_{yz} orbitals. The very large weight of this narrow energy distribution can be seen from DOS, and this distribution generates PF s smaller than those of SrTiO_3 (see Figs. 7(b), and 8(b)). This shows that a single or multiple very flat bands having large effective masses in all directions of Brillouin zone are not able to enhance TE performance, since the charge carriers associated to such flat bands are very localized and unable to participate in electronic transport. Increasing the quantum confinement in $(\text{SrTiO}_3)_5(\text{LaVO}_3)_1$ SL, also lowers the weight of narrow energy distribution and PF of these SL (see Figs. 7(b), and 8(b)).

C. Band structure engineering in $\text{AO}[\text{ABO}_3]_m$ naturally-ordered Ruddlesden-Popper phases

Highly anisotropic flat-and-dispersive bands can be found also in $\text{AO}[\text{ABO}_3]_m$ Ruddlesden-Popper naturally-ordered compounds. These compounds are formed from ABO_3 perovskite layers separated by an AO atomic layer and can nowadays be grown epitaxially with atomic-scale control.[87] To search for highly anisotropic bands, we have considered $\text{SrO}[\text{SrTiO}_3]_m$ ($m=1$ and 2) and $\text{SrO}[\text{SrCoO}_2\text{F}]_1$ compounds (Fig. 9). The insertion of SrO atomic layer in the crystallographic direction Oz creates the quantum confinement of electronic states in

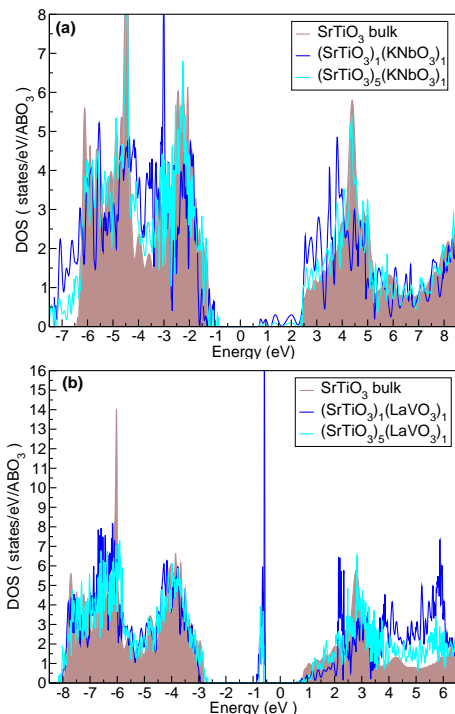


FIG. 7: (Color online) Total density of states (DOS) of: (a) $(\text{SrTiO}_3)_m(\text{KNbO}_3)_1$, and (b) $(\text{SrTiO}_3)_m(\text{LaVO}_3)_1$ superlattices ($m=1,5$) scaled to ABO_3 formula unit. DOS of bulk SrTiO_3 is also shown in background brown color.

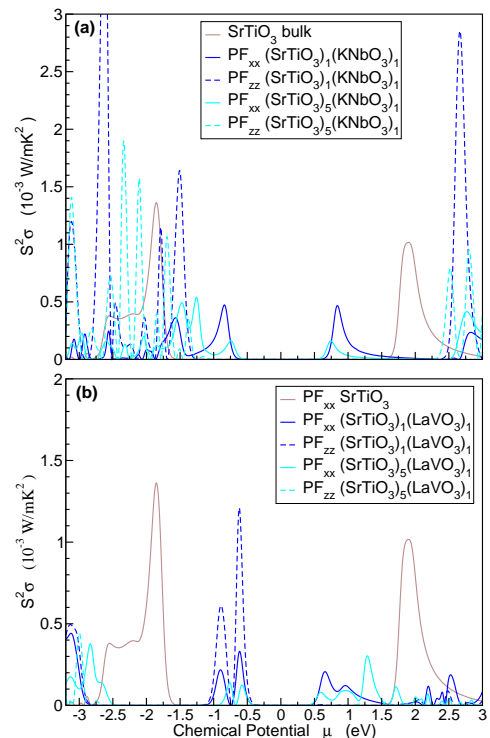


FIG. 8: (Color online) Power factor $PF = S^2\sigma$ dependence on chemical potential μ of: (a) $(\text{SrTiO}_3)_m(\text{KNbO}_3)_1$, and (b) $(\text{SrTiO}_3)_m(\text{LaVO}_3)_1$ superlattices ($m=1,5$) estimated at 300 K within B1-WC using the relaxation time $\tau = 0.43 \times 10^{-14}$ s.

ΓZ direction from the band structure of Sr_2TiO_4 and $\text{Sr}_3\text{Ti}_2\text{O}_7$ (see Fig. 10(a),(b)). It can be seen that CB bottom is formed by such very anisotropic bands, which generate narrow energy distributions with small weights (small length of ΓZ direction). The small weights of these distributions close to CB minimum (energy $\sim 1.75 - 2$ eV) can be seen more easily from scaled DOS per f.u. of

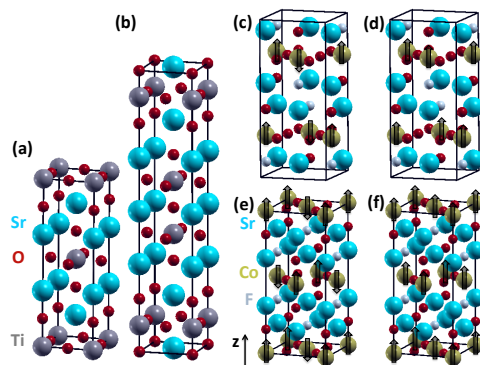


FIG. 9: (Color online) Structures of (a) Sr_2TiO_4 , and (b) $\text{Sr}_3\text{Ti}_2\text{O}_7$. Model structures of $\text{Sr}_2\text{CoO}_3\text{F}$ with: (c) AFM order on Co and one F atom in apical position, (d) FM order on Co and one F atom in apical position, (e) AFM order on Co and two F atoms in apical position, and (f) FM order on Co and two F atoms in apical position. The spin order on Co atoms is shown by arrows.

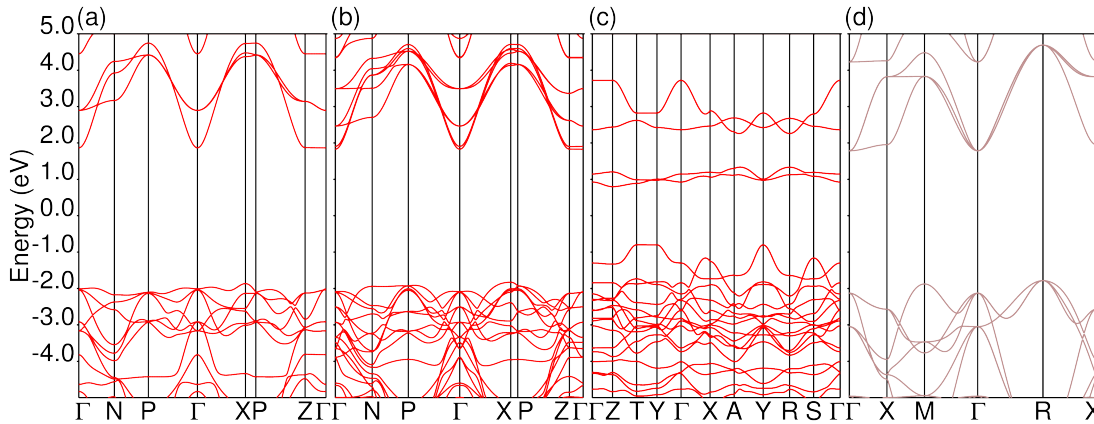


FIG. 10: Electronic band structure of: (a) Sr_2TiO_4 , (b) $\text{Sr}_3\text{Ti}_2\text{O}_7$, (c) $\text{Sr}_2\text{CoO}_3\text{F}$ (ground state structure from Fig. 9(c)), and (d) bulk SrTiO_3 estimated within B1-WC.

Sr_2TiO_4 and $\text{Sr}_3\text{Ti}_2\text{O}_7$, (Fig. 11(a)).

TE properties have been estimated using the same value of τ as that of bulk SrTiO_3 , because we want to compare the electronic contribution given by the electronic band structure of these naturally-ordered compounds to that of bulk SrTiO_3 . Due to the small weight of narrow energy distribution, the n-type PF corresponding to the chemical potential $\sim 1.75 - 2$ eV in Ox direction (PF_{xx}) is smaller than that of bulk SrTiO_3 (Fig. 12(a)). In the approximation that τ of $\text{SrO}[\text{SrTiO}_3]_m$ compounds is similar to that of bulk SrTiO_3 , the n-type PF is not improved.

From Co based $\text{AO}[\text{ABO}_3]_m$ compounds, we have explored the cobalt oxyfluoride $\text{Sr}_2\text{CoO}_3\text{F}$, in which F substitute O form apical position of CoO_6 octahedron.[88] In Figure 9(c-f) are shown the model structures in which F substitute one O atom (Fig. 9(c),(d)) or two O atoms (Fig. 9(e),(f)) form apical positions and Co atoms have AFM/FM order. The analysis of structural properties shows that the ground state structure is the structure in which F substitute one O atom form apical positions and Co atoms have AFM order (Fig. 9(c)). These results are in agreement with the experimental study, which finds G-type antiferromagnetic order of Co in $\text{Sr}_2\text{CoO}_3\text{F}$. [88] For the ground state structure, we studied the electronic and transport properties. The electronic band structure of $\text{Sr}_2\text{CoO}_3\text{F}$ contains two electronic bands with Co d orbital character in the (0.75eV, 1.25eV) energy interval (Fig. 10(c)). These bands do not have a very anisotropic character, requirement identified to maximize PF . [62] As a result the energy distribution of the two Co bands is narrow and has large weight, which can be seen from DOS (Fig. 11(b)). In the approximation that τ of $\text{Sr}_2\text{CoO}_3\text{F}$ is comparable to that of SrTiO_3 , the transport calculations show that PF of these compounds is smaller than that of SrTiO_3 (Fig. 12(b)).

D. Comparison of the different nanostructures with bulk SrTiO_3

In the approximation that τ of the considered nanostructures is comparable to that of bulk SrTiO_3 , none of the nanostructures shows higher TE performance than bulk SrTiO_3 , in spite of the fact that some of them possess highly anisotropic flat-and-dispersive TM d elec-

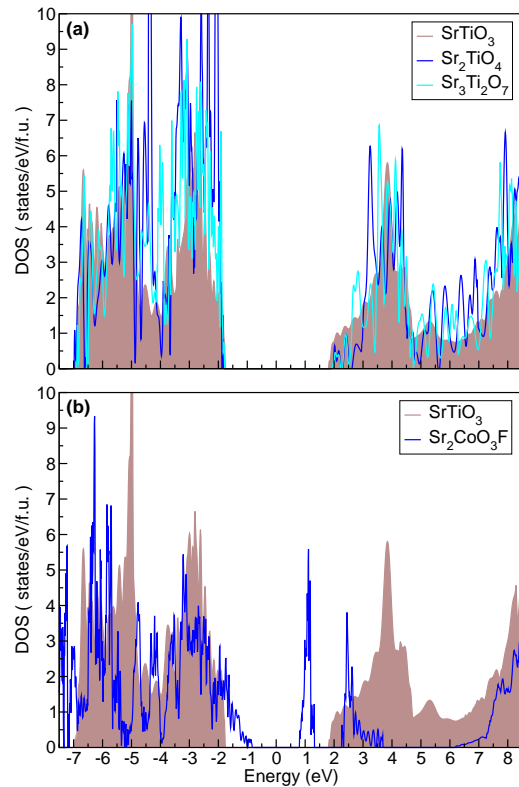


FIG. 11: (Color online) Total density of states (DOS) of: (a) Sr_2TiO_4 and $\text{Sr}_3\text{Ti}_2\text{O}_7$, and (b) $\text{Sr}_2\text{CoO}_3\text{F}$ (ground state structure from Fig. 9(c)) scaled to formula unit (f.u.= Sr_2TiO_4 , $\text{Sr}_{1.5}\text{TiO}_{3.5}$, and $\text{Sr}_2\text{CoO}_3\text{F}$, respectively).

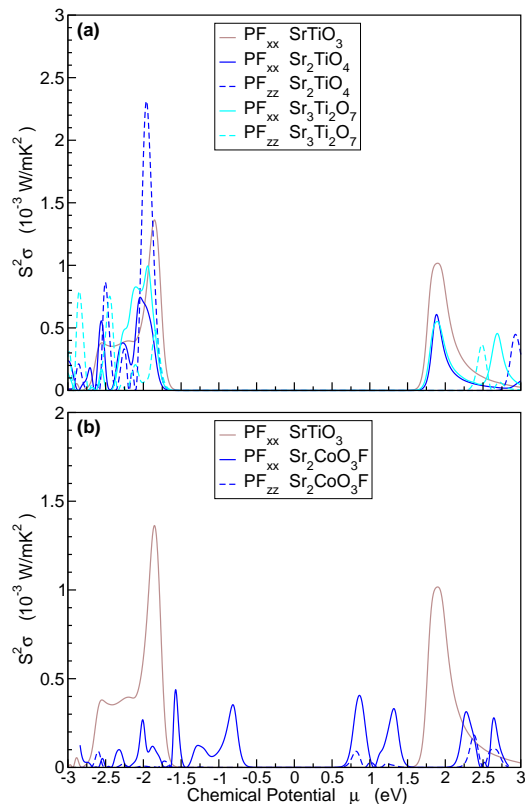


FIG. 12: (Color online) Power factor $PF = S^2\sigma$ dependence on chemical potential μ of: (a) Sr_2TiO_4 and $\text{Sr}_3\text{Ti}_2\text{O}_7$, and (c) $\text{Sr}_2\text{CoO}_3\text{F}$ naturally-ordered superlattices estimated at 300 K within B1-WC using the relaxation time $\tau = 0.43 \times 10^{-14}$ s.

tronic bands. In addition, the electronic states associated to these bands which participate in transport must have significant weights in order to maximize PF and n . The weights are proportional to DOS which depends on the density of states effective mass $m_d^* = \gamma^{2/3}(m_l^2 m_h)^{1/3}$, where γ is the carrier pocket degeneracy or band multiplicity.[89] Therefore in Table III, we show the estimated values of $\text{DOS}(\mu)/\text{f.u.}$ at the chemical potential μ which optimizes n- and p-type PF s, m_d^* , and band anisotropy ratio $R = m_h/m_l$. The usual anisotropic behavior is for heavy masses m_h across SL direction (Oz), and light masses m_l in the inplane SL direction (Ox , Oy). Although $(\text{SrTiO}_3)_1(\text{KNbO}_3)_1$ SL show very large R and large m_d^* values, their $\text{DOS}(\mu)/\text{f.u.}$ corresponding to the maximum n-type PF is about one order of magnitude smaller than that of SrTiO_3 . The confinement of Nb d_{xy} states achieved in these SL is able to create very large anisotropic electronic bands, but with small weights of the electronic states participating in transport due to their small carrier pocket volume in the Brillouin zone. $(\text{SrTiO}_3)_1(\text{LaVO}_3)_1$ SL at Z point of VB maximum, show unusual band anisotropic behavior with m_l along z direction and m_h along x and y directions, which gives large values for R , m_d^* , $\text{DOS}(\mu)/\text{f.u.}$ at the p-type PF maximum, and larger p-type power factor across SL direction (PF_{zz}) than along SL direction (PF_{xx}). Simi-

TABLE III: Heavy $m_h(m_e)$ and light $m_l(m_e)$ effective masses, anisotropy ratio R , carrier pocket degeneracy (or band multiplicity) γ , and density of states effective mass $m_d^*(m_e)$ for CB minima and VB maxima of SrTiO_3 and related superlattices, where m_e is free electron mass. $\text{DOS}(\mu)/\text{f.u.}$ (states/eV*f.u.) corresponding to μ which maximizes the n- or p-type PF s, where f.u. is ABO_3 , A_2BO_4 , or $\text{A}_{1.5}\text{BO}_{3.5}$ unit cell with only one TM atom per cell. The values for Fe_2TiSi are included for comparison.

		m_h	m_l	R	γ	m_d^*	$\text{DOS}(\mu)$
SrTiO_3	CB(Γ)	6.1	0.4	15.3	3	2.06	14.6
$(\text{SrTiO}_3)_1(\text{KNbO}_3)_1$	CB(Γ)	219.4	0.27	812.6	1	2.52	1.5
$(\text{SrTiO}_3)_1(\text{LaVO}_3)_1$	CB(Γ)	4.66	0.41	11.4	1	0.92	2.4
	VB(Z)	15.62	0.8	19.5	1	5.8	90.9
	VB(X)	13.92	1.73	8.1	1	3.47	
Sr_2TiO_4	CB(Γ)	74	0.42	176.2	1	2.36	4.7
$\text{Sr}_3\text{Ti}_2\text{O}_7$	CB(Γ)	50	0.4	125	1	2.0	4.9
$\text{Sr}_2\text{CoO}_3\text{F}$	CB(Z)	5.7	1.54	3.7	1	2.91	32
			2.8	2.0			
	VB(T)	244.6	0.36	679.4	1	3.65	5
			0.55	444.7			
Fe_2TiSi^a	CB(Γ)	90	0.2	450	3	3.19	31.2

^aFrom Ref. [62].

lar to $(\text{SrTiO}_3)_1(\text{KNbO}_3)_1$ SL, the confinement of Ti t_{2g} (d_{xy}) states participating in transport of Sr_2TiO_4 and $\text{Sr}_3\text{Ti}_2\text{O}_7$ naturally-ordered SL creates large anisotropy ratios, but at the same time detrimental reduced weights. On the other hand, Co t_{2g} (d_{xz} , and d_{yz}) states involved in the n-type transport of $\text{Sr}_2\text{CoO}_3\text{F}$ have large weights, but small anisotropy ratio. For comparison, we show in Table III the corresponding values for the full Heusler Fe_2TiSi which shows very large n-type PF s.[62] These very large PF s are achieved for concomitant large anisotropy ratio and weights, and small m_l effective mass which gives large carrier mobilities along the transport direction.

IV. CONCLUSIONS

Using the concept of electronic band structure engineering we tried to design materials possessing highly anisotropic electronic bands in $(\text{SrTiO}_3)_m(\text{KNbO}_3)_1$ and $(\text{SrTiO}_3)_m(\text{LaVO}_3)_1$ ($m=1$ and 5) artificial superlattices, and in $\text{SrO}[\text{SrTiO}_3]_m$ ($m=1$ and 2) and $\text{SrO}[\text{SrCoO}_2\text{F}]_1$ naturally-ordered superlattices. In spite of the fact that almost all superlattices possess such highly anisotropic electronic bands created by the confinement of TM d states, which is a signature of low-DET, their PF s are not better than that of SrTiO_3 . The origin of this TE performance is the small weights of electronic states participating in transport, which are associated to the highly anisotropic electronic bands. The experimental evidences for the decreased effective TE performance of

quantum wells and two-dimensional electron gas systems, caused by the contribution of barrier layers used to create the confinement, support our conclusion.[26, 90] Another detrimental effect on TE performance is the large m_l values along the transport direction of SrTiO₃ and related oxide materials, which are a factor ~ 2 larger than those of Fe based Heusler compounds [62], and a factor of ~ 16 larger than those of usual thermoelectrics such as PbTe.[89] If we account for the polaronic conductivity of SrTiO₃, these factors are ~ 3 times larger. Although SrTiO₃ possesses highly directional TM d electronic states active in transport, these states do not generate very large PF's. The origin of this TE performance is the low electron mobility as a result of the polaronic nature of electrical conductivity. In SrTiO₃ and related perovskite oxides, there is an important TM $d - O p$ hybridization with covalent character, which appears to

favour the polaronic conductivity. Binary TM oxides possessing high structural symmetries with stronger TM $d - d$ atomic interactions, may show high anisotropy, large weights and high mobilities of the charge carriers giving improved thermoelectric performance over ABO₃ perovskite oxides.

Acknowledgments

The authors acknowledge financial support from the Romanian National Authority for Scientific Research, CNCS-UEFISCDI, Project number PN-II-PT-PCCA-2013-4-1119. Ph. G. acknowledges the ARC project AIMED and the F.R.S.-FNRS project HiT4FiT.

-
- [1] S. Ohta et al., Appl. Phys. Lett. 2005, 87, 092108.
- [2] T. Okuda, K. Nakanishi, S. Miyasaka and Y. Tokura, Phys. Rev. B 2001, 63, 113104.
- [3] P.-P. Shang, B.-P. Zhang, Y. Liu, J.-F. Li, H.-M. Zhu, J. Electr. Mater. 2011, 40, 926.
- [4] H. C. Wang, C. I. Wang, W. B. Su, J. Liu, Y. Sun, H. Peng, L. M. Mei, JACS 2011, 94, 838.
- [5] J. Liu, C. L. Wang, Y. Li, W. B. Su, Y. H. Zhu, J. C. Li, and L. M. Mei, J. Appl. Phys. 2013, 114, 223714.
- [6] K. Park, J. S. Son, S. Ill Woo, K. Shin, M.-W. Oh, S.-D. Park, and T. Hyeon, J. Mater. Chem. A, 2014, 2, 4217.
- [7] A. V. Kovalevsky, A. A. Yaremchenko, S. Populoh, P. Thiel, D. P. Fagg, A. Weidenkaff, and J. R. Frade, Phys. Chem. Chem. Phys. 2014, 16, 26946.
- [8] M. T. Buscaglia et al., J. Eur. Ceram. Soc. 2014, 34, 307.
- [9] N. Wang, H. Chen, H. He, W. Norimatsu, M. Kusunoki, and K. Koumoto, Sci. Rep. 2013, 3, 3449.
- [10] B. Zhang, J. Wang, T. Zou, S. Zhang, X. Yaer, N. Ding, C. Liu, L. Miao, Y. Lia, and Y. Wu, J. Mater. Chem. C 2015, 3, 11406.
- [11] A. M. Dehkordi, S. Bhattacharya, T. Darroudi, X. Zeng, H. N. Alshareef, T. M. Tritt, J. Vis. Exp. 2015, 102, e52869.
- [12] Z. Lu, H. Zhang, W. Lei, D. C. Sinclair, and I. M. Reaney, Chem. Mater. 2016, 28, 925.
- [13] E. Li, N. Wang, H. He, and H. Chen, Nanosc. Res. Lett. 2016, 11, 188.
- [14] Y. Wang, K. H. Lee, H. Ohta, and K. Koumoto, J. Appl. Phys. 2009, 105, 103701.
- [15] I. Matsubara et al. Appl. Phys. Lett. 2001, 78, 3627.
- [16] M. Ohtaki, T. Tsubota and K. Egushi, J. Appl. Phys. 1996, 79, 1816.
- [17] T. Tsubota, M. Ohtaki, K. Eguchi, and H. Arai, J. Mater. Chem. 1997, 7, 85.
- [18] Z.-H. Wu, H.-Q. Xie, and Q.-F. Zeng, J. Inorg. Mater. 2013, 28, 921.
- [19] S. Saini, P. Mele, H. Honda, K. Matsumoto, K. Miyazaki, and A. Ichinose, J. Electr. Mater. 2014, 43, 2145.
- [20] Z. H. Wu, H. Q. Xie, and Y. B. Zhai, J. Nanosci. Nanotechnol. 2015, 15, 3147.
- [21] J.-L. Lan, Y. Liu, Y.-H. Lin, C.-W. Nan, Q. Cai, and X. Yang, Sci. Rep. 2015, 5, 7783.
- [22] S. F. Wang, F. Q. Liu, Q. Lu, S. Y. Dai, J. L. Wang, W. Yu, G. S. Fu, J. Eur. Ceram. Soc. 2013, 33, 1763.
- [23] X. R. Zhang, H. L. Li, and J. L. Wang, J. Adv. Ceram. 2015, 4, 226.
- [24] M. Backhaus-Ricoult, J. Rustad, L. Moore, C. Smith, and J. Brown, Appl. Phys. A 2014, 116, 433.
- [25] A. C. Masset et al., Phys. Rev. B 2000, 62, 166.
- [26] H. Ohta et al., Nature Materials 2007, 6, 129.
- [27] J. Sui, J. Li, J. He, Y.-L. Pei, D. Berardan, H. Wu, N. Dragoe, W. Caia, and L.-D. Zhao, Energy Environ. Sci. 2013, 6, 2916.
- [28] H. Ohta, K. Sugiura and K. Koumoto, Inorg. Chem. 2008, 47, 8429.
- [29] K. Koumoto, I. Terasaki and R. Funahashi, MRS Bulletin 2006, 31, 206.
- [30] Y. Mune et al. Appl. Phys. Lett. 2007, 91, 192105.
- [31] P. Garcia-Fernandez, M. Verissimo-Alves, D. I. Bilc, P. Ghosez, and J. Junquera, Phys. Rev. B 2012, 86, 085305.
- [32] R. Astala and P. D. Bristowe, J. Phys.: Condens. Matter 2002, 14, L149.
- [33] X. G. Guo et al., Phys. Lett. A 2003, 317, 501.
- [34] C. Zhang et al., Mat. Chem. Phys. 2008, 107, 215.
- [35] J. N. Yun and Z. Y. Zhang, Chin. Phys. B 2009, 18, 2945.
- [36] H. Usui et al., Phys. Rev. B 2010, 81, 205121.
- [37] R. Zhang et al., J. Am. Ceram. Soc. 2010, 93, 1677.
- [38] A. Kinaci, C. Sevik, and T. Çağın, Phys. Rev. B 2010, 82, 155114.
- [39] J. D. Baniecki1, M. Ishii, H. Aso, K. Kurihara, and D. Ricinschi, J. Appl. Phys. 2013, 113, 013701.
- [40] D. F. Zou, Y. Y. Liu, S. H. Xie, J. G. Lin, J. Y. Li, Chem. Phys. Lett. 2013, 586, 159.
- [41] K. Shirai and K. Yamanaka, J. Appl. Phys. 2013, 113, 053705.
- [42] M. U. Kahaly, and U. Schwingenschlöggl, J. Mater. Chem. A 2014, 2, 10379.
- [43] K. Singsoog, T. Seetawan, A. Vora-Ud, and C. Thanachayanont, Integr. Ferroelectr. 2014, 155, 111.
- [44] R.-Z. Zhang, X.-Y. Hu, P. Guo, C.-l. Wang, Phys. B - Cond. Matter. 2012, 407, 1114.
- [45] A. Roy, Phys. Rev. B 2016, 93, 100101.

- [46] B. Himmetoglu and A. Janotti, *J. Phys.: Condens. Matter* 2016, 28, 065502.
- [47] B. Khan, H. A. R. Aliabad, N. Razghandi, M. Maqbool, S. J. Asadabadi, and I. Ahmad, *Comput. Phys. Commun.* 2015, 187, 1.
- [48] F. P. Zhang et al., *Physica B: Condens. Matter* 2011, 406, 1258.
- [49] F. P. Zhang et al., *J. Phys. Chem. Sol.* 2013, 74, 1859.
- [50] M. Molinari, D. A. Tompsett, S. C. Parker, F. Azough, and R. Freer, *J. Mater. Chem. A* 2014, 2, 14109.
- [51] X. H. Zhang et al., *J. Alloy. Compd.* 2015, 634, 1.
- [52] P. Srepusharawoot, S. Pinitsoontorn, and S. Maensiri, *Comput. Mater. Sci.* 2016, 114, 64.
- [53] K. P. Ong, D. J. Singh, P. Wu, *Phys. Rev. B* 2011, 83, 115110.
- [54] X. Qua, W. Wanga, S. Lv, D. Jia, *Solid State Commun.* 2011, 151, 332.
- [55] S. Jantrasee, S. Pinitsoontorn, and P. Moontragoon, *J. Electr. Mater.* 2014, 43, 1689.
- [56] A. Alvarado, J. Attapattu, Y. Zhang, C. F. Chen, *J. Appl. Phys.* 2015, 118, 165101.
- [57] Z. Huang, T. Y. Lu, H. Q. Wang, J. C. Zheng, *AIP Adv.* 2015, 5, 097204.
- [58] X. Chen, D. Parker, M. H. Du, and D. J. Singh, *New J. Phys.* 2013, 15, 043029.
- [59] L. Lindsay and D. S. Parker, *Phys. Rev. B* 2015, 92, 144301.
- [60] D. Bayerl and E. Kioupakis, *Phys. Rev. B* 2015, 91, 165104.
- [61] Y. Chumakov et al., *J. Electr. Matter.* 2013, 42, 1597.
- [62] D. I. Bilc, G. Hautier, D. Waroquiers, G.-M. Rignanese, and Ph. Ghosez, *Phys. Rev. Lett.* 2015, 114, 136601.
- [63] K. Biswas et al., *Nature* 2012, 489, 414.
- [64] J. P. Heremans, M. S. Dresselhaus, L. E. Bell, and D. T. Morelli, *Nature Nanotech.* 2013, 8, 471.
- [65] F. Inaba et al., *Phys. Rev. B* 1995, 52, 2221.
- [66] Q. Wang et al., *Sci. Technol. Adv. Mat.* 2004, 5, 543.
- [67] D. I. Bilc, R. Orlando, R. Shaltaf, G.-M. Rignanese, Jorge Iniguez and Ph. Ghosez, *Phys. Rev. B* 2008, 77, 165107.
- [68] M. Goffinet, P. Hermet, D. I. Bilc, and Ph. Ghosez, *Phys. Rev. B* 2009, 79, 014403.
- [69] A. Prikockyte, D. Bilc, P. Hermet, C. Dubourdieu, and Ph. Ghosez, *Phys. Rev. B* 2011, 84, 214301.
- [70] J. P. Perdew and A. Zunger, *Phys. Rev. B* 1981, 23, 5048.
- [71] J. P. Perdew, K. Burke, and M. Ernzerhof, *Phys. Rev. Lett.* 1996, 77, 3865.
- [72] Z. Wu and R. E. Cohen, *Phys. Rev. B* 2006, 73, 235116.
- [73] R. Dovesi, R. Orlando, B. Civalleri, C. Roetti, V. R. Saunders, and C. M. Zicovich-Wilson, *Z. Kristallogr.* 2005, 220, 571.
- [74] T. Bredow, P. Heitjans, M. Wilkening, *Phys. Rev. B* 2004, 70, 115111.
- [75] S. Piskunov, E. Heifets, R. I. Eglitis, and G. Borstel, *Comp. Mat. Sci.* 2004, 29, 165.
- [76] R. Dovesi, C. Roetti, C. Freyria Fava, M. Prencipe, and V.R. Saunders, *Chem. Phys.* 1991, 156, 11.
- [77] M. F. Peintinger, D. Vilela Oliveira, and T. Bredow, *J. Comput. Chem.* 2013, 34, 451.
- [78] W. C. Mackrodt, N. M. Harrison, V. R. Saunders, N. L. Allan, M. D. Towler, E. Apra, and R. Dovesi, *Phil. Mag. A* 1993, 68, 653.
- [79] X. Cao, M. Dolg, *J. Molec. Struct. (Theochem)* 2002, 581, 139.
- [80] G. K. H. Madsen and D. J. Singh, *Comput. Phys. Commun.* 175, 67 (2006).
- [81] H. Muta, K. Kurosaki, S. Yamanaka, *J. Alloys Comp.* 2005, 392, 306.
- [82] K. H. Hellwege, and A. M. Hellwege (Eds.), *Ferroelectrics and Related Substances, New Series, vol. 3, Landolt-Bornstein*, Springer Verlag, Berlin, 1969, group III.
- [83] K. van Benthem, C. Elsasser, and R. H. French, *J. Appl. Phys.* 2001, 90, 6156.
- [84] S. Ohta, T. Nomura, H. Ohta and K. Koumoto, *J. Appl. Phys.* 2005, 97, 034106.
- [85] J. L. M. van Mechelen, D. van der Marel, C. Grimaldi, A. B. Kuzmenko, N. P. Armitage, N. Reyren, H. Hagemann, and I. I. Mazin, *Phys. Rev. Lett.* 2008, 100, 226403.
- [86] Y. Pei, A. D. LaLonde, H. Wang, and G. J. Snyder, *Energy Environ. Sci.* 2012, 5, 7963.
- [87] Y. F. Nie, Y. Zhu, C.-H. Lee, L. F. Kourkoutis, J. A. Mundy, J. Junquera, Ph. Ghosez, D. J. Baek, S. Sung, X. X. Xi, K. M. Shen, D. A. Muller, and D. G. Schlom, *Nature Commun.* 2014, 5, 4530.
- [88] Y. Tsujimoto et al., *Inorg. Chem.* 2012, 51, 4802.
- [89] D. I. Bilc, S. D. Mahanti, and M. G. Kanatzidis, *Phys. Rev. B* 2006, 74, 125202.
- [90] L. D. Hicks, T. C. Harman, X. Sun, and M. S. Dresselhaus, *Phys. Rev. B* 1996, 53, R10493.